

Growth of compositionally uniform $\text{In}_x\text{Ga}_{1-x}\text{N}$ layers with low relaxation degree on GaN by molecular beam epitaxy

Jingxuan Kang, Mikel Gómez Ruiz, Duc Van Dinh, Aidan F Campbell, Philipp John, Thomas Auzelle, Achim Trampert, Jonas Lähnemann, Oliver Brandt, and Lutz Geelhaar^{a)}

Paul-Drude-Institut für Festkörperelektronik, Leibniz-Institut im Forschungsverbund Berlin e.V., Hausvogteiplatz 5–7, 10117 Berlin, Germany.

500-nm-thick $\text{In}_x\text{Ga}_{1-x}\text{N}$ layers with $x = 0.05\text{--}0.14$ are grown using plasma-assisted molecular beam epitaxy, and their properties are assessed by a comprehensive analysis involving x-ray diffraction, secondary ion mass spectrometry, and cathodoluminescence as well as photoluminescence spectroscopy. We demonstrate low degrees of strain relaxation (10% for $x = 0.12$), low threading dislocation densities ($1 \times 10^9 \text{ cm}^{-2}$ for $x = 0.12$), uniform composition both in the growth and lateral direction, and a narrow emission band. The unique sum of excellent materials properties make these layers an attractive basis for the top-down fabrication of ternary nanowires.

The ternary alloy $\text{In}_x\text{Ga}_{1-x}\text{N}$ is arguably the most important optoelectronic material since it covers the wide spectral range from the near-infrared to the entire visible region and has enabled ubiquitous solid-state lighting.¹ In particular, $\text{In}_x\text{Ga}_{1-x}\text{N}$ quantum wells emitting blue light exhibit internal quantum efficiencies approaching unity thanks to mature growth procedures.² At the same time, the level of material quality is still substantially lower for quantum wells with higher In content and layers with a thickness exceeding a few hundred nanometers. The central challenge in this context is the lattice mismatch to GaN templates and the lack of better-suited substrates. Specifically, during the growth of thick layers with low to moderate In content, strain relaxes gradually which in turn leads to increasing In incorporation, a phenomenon called ‘compositional pulling’.^{3,4} Moreover, strain relaxation is associated with the formation of threading dislocations (TDs) which act as non-radiative recombination centers.^{5,6}

The growth of $\text{In}_x\text{Ga}_{1-x}\text{N}$ layers with thickness on the order of hundreds of nanometers is mainly motivated by two purposes: First, such layers could serve as pseudo-substrates for the growth of $\text{In}_x\text{Ga}_{1-x}\text{N}$ quantum wells with high In content emitting, e. g., in the red spectral region.^{7,8} Second, such layers could be used as active region in optoelectronic converters such as photodetectors and solar cells.^{9,10} While both purposes require thick layers, the required properties differ significantly. The use as pseudo-substrate necessitates a high degree of strain relaxation to provide a template with low mismatch to the desired quantum wells with high In content. In contrast, for the active region of light-absorbing devices,^{11–13} a low degree of strain relaxation is crucial to avoid TDs and other defects reducing quantum efficiency.⁶ Furthermore, in the second case a spatially highly homogeneous In content is typically desirable, whereas compositional gradients in the growth direction do not impede the functionality of pseudo-substrates and may actually be introduced on purpose.

A third, new motivation for thick $\text{In}_x\text{Ga}_{1-x}\text{N}$ layers is to employ them as the starting point for the top-down fabrication of $\text{In}_x\text{Ga}_{1-x}\text{N}$ nanowires. The nanowire geometry offers conceptual advantages for optoelectronic applications based

on light absorption such as photocatalytic water splitting.¹⁴ In particular, light can be absorbed more efficiently than in thin layers, and charge carriers can be collected in the direction orthogonal to the impinging light, thus reducing the distance from the active region. However, in the bottom-up growth of $\text{In}_x\text{Ga}_{1-x}\text{N}$ nanowires, the resulting morphology is strongly coupled to the chosen composition and doping.^{15,16} In contrast, in a top-down approach the former is defined during etching, and the latter during initial planar epitaxy.

The layer requirements for subsequent top-down nanowire fabrication resemble those of layers serving as light-absorbing active region in that compositional uniformity is desirable and structural defects should be avoided. In particular, top-down nanowires could inherit TDs from the original layer, which would significantly reduce the nanowire quantum efficiency. Under the assumption that the TDs are randomly distributed in the layer, the number n of TDs in top-down nanowires is statistically determined by the density ρ of TDs in the layer as well as the nanowire diameter d : $n = d^2\pi\rho/4$. Thus, it is expected that a planar $\text{In}_x\text{Ga}_{1-x}\text{N}$ layer with TD density of approximately $1 \times 10^9 \text{ cm}^{-2}$ will yield a nanowire ensemble comprising $\geq 98\%$ TD-free nanowires if $d \leq 50 \text{ nm}$.¹⁷

This study targets the growth of thick $\text{In}_x\text{Ga}_{1-x}\text{N}$ layers suitable for the subsequent top-down fabrication into nanowires. We employ plasma-assisted molecular beam epitaxy (PA-MBE) to grow $\text{In}_x\text{Ga}_{1-x}\text{N}$ layers with a thickness of 500 nm and In contents of up to 0.14. Systematic examination of their structural and optical properties demonstrates a low relaxation degree and correspondingly low density of TDs, uniform composition, and a narrow photoluminescence (PL) emission band.

$\text{In}_x\text{Ga}_{1-x}\text{N}$ layers with a thickness of 500 nm were grown using PA-MBE on commercial GaN(0001) templates at a substrate temperature of 620 °C. Two In cells were employed, one of which served to compensate In desorption and maintain intermediate In-rich growth conditions, the other one to incorporate In for the desired stoichiometry. Before growth, In cell A was set to a flux of $3.2 \times 10^{14} \text{ cm}^{-2}\text{s}^{-1}$, sufficient for the accumulation of In droplets on the surface. The time necessary for droplet formation was monitored by reflection high-energy electron diffraction (RHEED),¹⁸ as explained in more detail in the supplementary material, and used as an indicator for the actual substrate temperature.¹⁹ Next, the flux of

^{a)}Electronic email: Geelhaar@pdi-berlin.de

In cell A was adjusted to ensure intermediate In-rich growth conditions.¹⁹ The cell shutter was opened and closed again after 60 s, and the In cell A temperature was fine-tuned utilizing RHEED intensity transients to ensure the formation of an In adlayer.¹⁸ After these adjustments and full In desorption, all four shutters were opened. For the growth of $\text{In}_{0.12}\text{Ga}_{0.88}\text{N}$, the fluxes of In cell B, Ga, and N were $5.8 \times 10^{13} \text{ cm}^{-2}\text{s}^{-1}$, $5.5 \times 10^{14} \text{ cm}^{-2}\text{s}^{-1}$, and $6.1 \times 10^{14} \text{ cm}^{-2}\text{s}^{-1}$, respectively. In terms of the $\text{In}_x\text{Ga}_{1-x}\text{N}$ layer stoichiometry, in addition to the In cell B flux, the decomposition of $\text{In}_x\text{Ga}_{1-x}\text{N}$ during the epitaxy process, which depends on the growth temperature as well as In composition, also affects the final In content of the epitaxial layers.²⁰ For $\text{In}_x\text{Ga}_{1-x}\text{N}$ layers with different In concentration, the metal flux of In cell B and Ga was adjusted accordingly.

After growth, the morphology of the $\text{In}_x\text{Ga}_{1-x}\text{N}$ layers was evaluated using RHEED and atomic force microscopy (AFM). Subsequently, a triple-axis high resolution x-ray diffractometer (Philips PANalytical X'Pert PRO MRD) equipped with a two-bounce hybrid $\text{Ge}(220)$ monochromator and a $\text{CuK}_{\alpha 1}$ source ($\lambda = 1.540598 \text{ \AA}$) was employed to reveal the structural properties of the $\text{In}_x\text{Ga}_{1-x}\text{N}$ layers. The In content and strain relaxation degree were determined based on $2\theta - \omega$ scans of the 0002, 0004, 10 $\bar{1}$ 2, 10 $\bar{1}$ 3, 11 $\bar{2}$ 2, and 20 $\bar{2}$ 1 reflections as well as reciprocal space maps (RSM) around the 10 $\bar{1}$ 5 reflection.^{21,22} Moreover, to evaluate the structural quality of the $\text{In}_x\text{Ga}_{1-x}\text{N}$ layers, rocking curves were acquired around the 0002 and 10 $\bar{1}$ 2 reflections. The TD density was extracted separately from maps of the panchromatic cathodoluminescence (CL) intensity obtained at 10 K and transmission electron microscopy (TEM) measurements. Hyperspectral CL maps and secondary ion mass spectrometry (SIMS) were utilized to evaluate the compositional uniformity. Quantitative information about the In content was obtained from the SIMS measurements by comparison with a reference $\text{In}_x\text{Ga}_{1-x}\text{N}$ layer whose composition was calibrated using Rutherford backscattering spectrometry. PL spectra were measured at room temperature using a Renishaw InVia setup to investigate the emission properties. The samples were excited by a 325 nm He-Cd laser with a spot diameter of about 1 μm and an excitation density of $\approx 1 \text{ kW cm}^{-2}$.

The RHEED pattern of the $\text{In}_{0.12}\text{Ga}_{0.88}\text{N}$ layer after growth presented in Fig. 1(a) reveals the $\sqrt{3} \times \sqrt{3} \text{ R}30^\circ$ surface reconstruction known to reflect an In-terminated surface^{23,24} and exhibits sharp streaks that indicate a smooth surface. Consistently, the corresponding AFM topograph in Fig. 1(b) shows the typical hexagonal pyramids characteristic for $\text{In}_x\text{Ga}_{1-x}\text{N}$ grown by PA-MBE.^{25,26} The monolayer spiral growth around screw threading dislocations is well resolved, and the root-mean-square roughness extracted over a scanning area of $3 \times 3 \mu\text{m}^2$ is 1.9 nm. The smooth surface, absence of ∇ -pits, and the observation of the $\sqrt{3} \times \sqrt{3} \text{ R}30^\circ$ reconstruction confirm that the $\text{In}_x\text{Ga}_{1-x}\text{N}$ layer was grown under In-stable conditions with an In adlayer with > 1 monolayer coverage.²⁷

Figure 2(a) and 2(b) display for the $\text{In}_{0.12}\text{Ga}_{0.88}\text{N}$ layer x-ray diffraction (XRD) ω scans of the 0002 and 10 $\bar{1}$ 2 reflection. The profiles exhibit full widths at half maximum

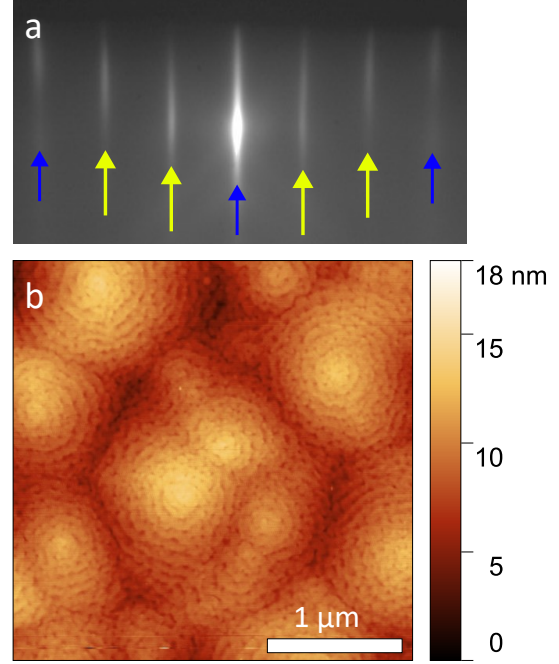


FIG. 1. (a) RHEED pattern of the $\text{In}_{0.12}\text{Ga}_{0.88}\text{N}$ surface after growth along the $[1\bar{1}00]$ azimuth showing the $\sqrt{3} \times \sqrt{3} \text{ R}30^\circ$ reconstruction induced by the In adlayer with integer and fractional reflections marked by blue and yellow arrows, respectively. (b) AFM topograph of the $\text{In}_{0.12}\text{Ga}_{0.88}\text{N}$ layer.

(FWHM) of $417''$ and $633''$, respectively. These FWHM values are larger than the GaN template, which are $286''$ and $449''$ respectively, yet are comparable to the FWHM reported for PA-MBE grown $\text{In}_x\text{Ga}_{1-x}\text{N}$ ($x = 0.12$) on a GaN template,²⁸ as well as for strain-relaxed $\text{In}_x\text{Ga}_{1-x}\text{N}$ pseudo-substrate with lower In content $x < 0.1$ obtained from strained $\text{In}_x\text{Ga}_{1-x}\text{N}$ layer transfer⁷ with thicknesses less than the 500 nm of our $\text{In}_{0.12}\text{Ga}_{0.88}\text{N}$ layer. The RSM in Fig. 2(c) reveals for this layer $x = 0.12$ and a relaxation degree of only 10%. This In content and strain relaxation degree are consistent with the results calculated from the average lattice constant which is determined from $2\theta - \omega$ scans of the 0002, 0004, 10 $\bar{1}$ 2, 10 $\bar{1}$ 3, 11 $\bar{2}$ 2, and 20 $\bar{2}$ 1 reflections.²¹ The 10% strain relaxation degree of our $\text{In}_{0.12}\text{Ga}_{0.88}\text{N}$ layer is on the lower end compared to reported values for epitaxial $\text{In}_x\text{Ga}_{1-x}\text{N}$ layers with similar thickness and In content grown on GaN templates.²⁸⁻³⁰

Direct insight into the TD density is provided by panchromatic CL intensity maps as depicted in Fig. 2(d). In addition to minor fluctuations across the surface, there are dark spots indicating positions of strongly reduced intensity that are the outcrops of TDs at the surface.⁶ Averaging over different locations on the $\text{In}_{0.12}\text{Ga}_{0.88}\text{N}$ layer, we obtained a TD density of $\approx 1 \times 10^9 \text{ cm}^{-2}$. For comparison, the TD density of the GaN (0001) template, determined using the same method before growth, is $\approx 2 \times 10^8 \text{ cm}^{-2}$. The TD density of the $\text{In}_{0.12}\text{Ga}_{0.88}\text{N}$ layer was confirmed by transmission electron microscopy measurements (not shown). We note that the TD

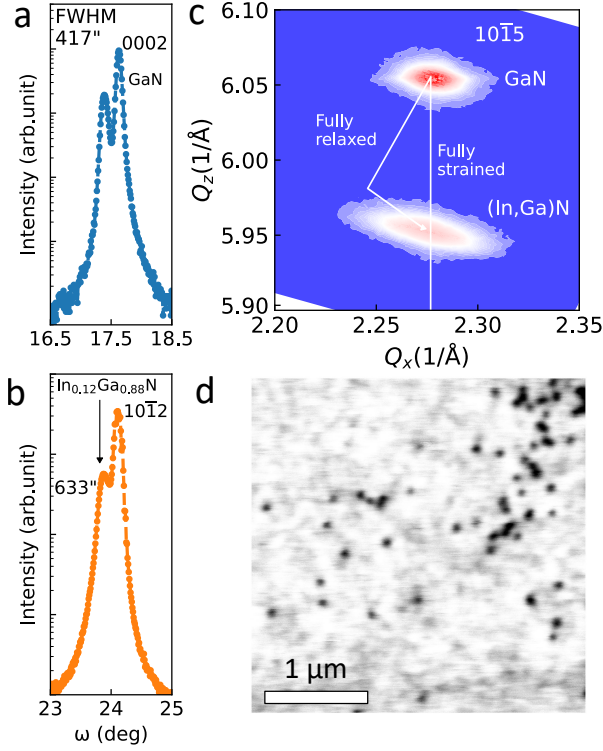


FIG. 2. XRD ω scans of the $\text{In}_{0.12}\text{Ga}_{0.88}\text{N}$ sample around the (a) 0002 and (b) $10\bar{1}2$ reflections performed with an open detector. (c) RSM around the GaN $10\bar{1}5$ reflection revealing an In content of 0.12. (d) Panchromatic CL intensity map acquired at 10 K. The dark spots correspond to TDs.

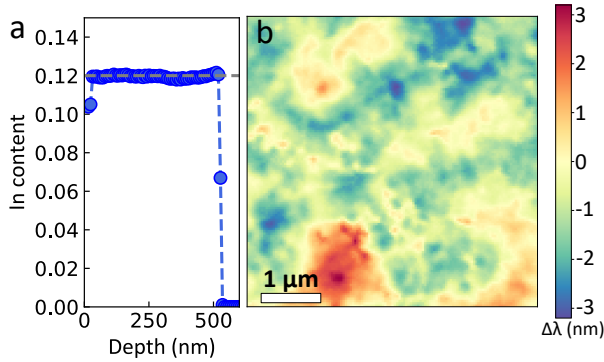


FIG. 3. (a) In content depth profile obtained by SIMS. (b) Room temperature map of the variation of the CL peak emission wavelength.

density is as low as the reported values for similar layers in literature^{29,31} and is consistent with the low strain relaxation degree determined by XRD.

The spatial homogeneity of the In content is another factor critical for $\text{In}_x\text{Ga}_{1-x}\text{N}$ to be used as active region in devices. A depth profile of the In content in our $\text{In}_{0.12}\text{Ga}_{0.88}\text{N}$ layer was obtained by SIMS, and the result is presented in Fig. 3(a).

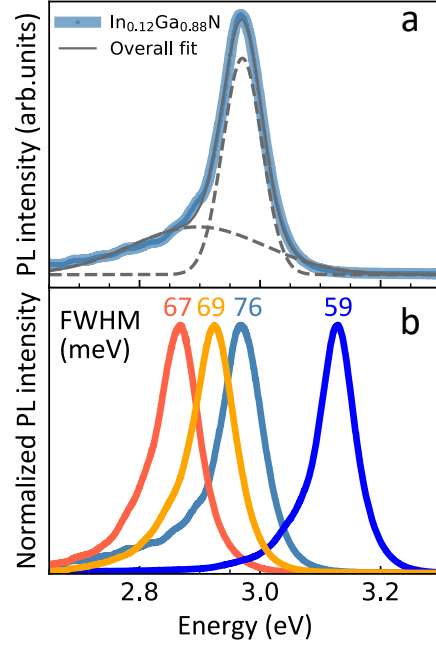


FIG. 4. (a) Room temperature PL spectrum (broad turquoise line) of the $\text{In}_{0.12}\text{Ga}_{0.88}\text{N}$ layer fitted (grey solid line) with two Gaussians (dashed grey lines). (b) Room temperature PL spectra of thick $\text{In}_x\text{Ga}_{1-x}\text{N}$ layers with In content ranging from 0.05 to 0.14.

The In content remains constant along the growth direction throughout the entire layer. In contrast, during the growth of thick $\text{In}_x\text{Ga}_{1-x}\text{N}$ layers the In content often increases due to compositional pulling.^{4,28} The high uniformity in the growth direction found here is a direct consequence of the low strain relaxation degree of our $\text{In}_{0.12}\text{Ga}_{0.88}\text{N}$ layer. To assess the compositional homogeneity in the lateral direction, maps of the CL peak emission wavelength were acquired, as depicted in Fig. 3(b). Within this area of $5 \times 5 \mu\text{m}^2$, the variation of the peak emission wavelength amounts to ± 3 nm, indicating that there are only negligible fluctuations in In content on the local scale ($< 0.8\%$). The combination of SIMS and hyperspectral CL maps demonstrates that our $\text{In}_{0.12}\text{Ga}_{0.88}\text{N}$ layer exhibits a uniform In content both in the growth and lateral direction.

Room temperature PL spectroscopy is another way to assess the compositional uniformity of the $\text{In}_x\text{Ga}_{1-x}\text{N}$ samples. The spectrum of the $\text{In}_{0.12}\text{Ga}_{0.88}\text{N}$ layer is depicted in Fig. 4(a). The spectrum is comparably narrow but its shape indicates the presence of two distinct emission bands. Fitting with two Gaussians results in peak energies of 2.97 and 2.89 eV. The band at 2.97 eV corresponds to the recombination of (presumably localized) excitons, while the other one is attributed to the first LO replica. Note that the spectral separation of the zero phonon line and the first LO replica does not equal the LO energy due to their different density of states, which introduces a shift proportional to kT .³² The FWHM of the excitonic emission resulting from the Gaussian fit is 76 meV, suggesting a low degree of alloy disorder

within the sample.^{33,34}

So far, we have focused on the $\text{In}_x\text{Ga}_{1-x}\text{N}$ layer with 0.12 In content. In addition, a series of samples with measured In content spanning from 0.05 to 0.14 was grown under identical conditions, the only variation being the In/Ga flux ratio. The corresponding PL spectra are shown in Fig. 4(b) and reveal a monotonic red shift from 3.13 to 2.87 eV with increasing In content. In parallel, the FWHM values are all in range 60 to 76 meV. Data for the structural analysis of the sample whose PL emission is centered at 2.87 eV is presented in the supporting information. In short, we extracted an In content of 0.14, a strain relaxation degree of 20%, a TD density of $1.9 \times 10^9 \text{ cm}^{-2}$, and an almost uniform In content in the growth direction.

Compared to the $\text{In}_{0.12}\text{Ga}_{0.88}\text{N}$ layer, the higher In content of 0.14 leads to more plastic strain relaxation and accordingly a higher TD density. At the same time, the FWHMs of the PL spectra do not differ much between the different samples. In general, spectral broadening is attributed to $\text{In}_x\text{Ga}_{1-x}\text{N}$ alloy disorder.^{33,34} Thus, our sample series feature very uniform composition. We emphasize that for all of our samples the PL FWHMs are comparable to the best values reported in literature for layers with similar In contents and thicknesses.^{35–37}

In summary and conclusion, we have demonstrated the growth of 500-nm-thick $\text{In}_x\text{Ga}_{1-x}\text{N}$ layers with In contents up to 0.14 that combine various desirable properties. In particular, the relaxation degree and the TD density are low, the compositional uniformity is high, and the PL emission band is narrow. These layers present an excellent starting point for the top-down fabrication of $\text{In}_x\text{Ga}_{1-x}\text{N}$ nanowire ensembles with highly uniform properties and high quantum efficiency. It is expected that $\geq 96\%$ of top-down nanowires fabricated from the $\text{In}_x\text{Ga}_{1-x}\text{N}$ layer with $x = 0.14$ are free of TDs if the mean nanowire diameter is 50 nm.

The authors thank Hans-Peter Schönherr for technical support and Andrea Ardenghi for critically reading the manuscript. This work has been supported by Deutsche Forschungsgemeinschaft under grants Ge2224/6-1 and Au610/1-1.

- ¹F. K. Yam and Z. Hassan, “InGaN: An overview of the growth kinetics, physical properties and emission mechanisms,” *Superlattices and Microstructures* **43**, 1–23 (2008).
- ²S. Nakamura, T. Mukai, and M. Senoh, “Candela-class high-brightness InGaN/AlGaN double-heterostructure blue-light-emitting diodes,” *Applied Physics Letters* **64**, 1687–1689 (1994).
- ³T. Schulz, L. Lymperakis, M. Anikeeva, M. Siekacz, P. Wolny, T. Markurt, and M. Albrecht, “Influence of strain on the indium incorporation in (0001) GaN,” *Phys. Rev. Mater.* **4**, 073404 (2020).
- ⁴S. Pereira, M. R. Correia, E. Pereira, K. P. O’Donnell, C. Trager-Cowan, F. Sweeney, and E. Alves, “Compositional pulling effects in $\text{In}_x\text{Ga}_{1-x}\text{N}/\text{GaN}$ layers: A combined depth-resolved cathodoluminescence and Rutherford backscattering/channeling study,” *Phys. Rev. B* **64**, 205311 (2001).
- ⁵J. S. Speck and S. J. Rosner, “The role of threading dislocations in the physical properties of GaN and its alloys,” *Physica B: Condensed Matter* **273–274**, 24–32 (1999).
- ⁶J. Lähnemann, V. M. Kaganer, K. K. Sabelfeld, A. E. Kireeva, U. Jahn, C. Chêze, R. Calarco, and O. Brandt, “Carrier Diffusion in GaN: A Cathodoluminescence Study. III. Nature of Nonradiative Recombination at Threading Dislocations,” *Phys. Rev. Appl.* **17**, 024019 (2022).
- ⁷A. Even, G. Laval, O. Ledoux, P. Ferret, D. Sotta, E. Guiot, F. Levy, I. C. Robin, and A. Dussaigne, “Enhanced In incorporation in full InGaN het-

- erostructure grown on relaxed InGaN pseudo-substrate,” *Applied Physics Letters* **110**, 262103 (2017).
- ⁸K. Ema, R. Hieda, and H. Murakami, “Growth of lattice-relaxed InGaN thick films on patterned sapphire substrates by tri-halide vapor phase epitaxy,” *Jpn. J. Appl. Phys.* **60**, 105501 (2021).
- ⁹A. G. Bhuiyan, K. Sugita, A. Hashimoto, and A. Yamamoto, “InGaN Solar Cells: Present State of the Art and Important Challenges,” *IEEE J. Photovolt.* **2**, 276–293 (2012).
- ¹⁰D. Kong, Y. Zhou, J. Chai, S. Chen, L. Chen, L. Li, T. Lin, W. Wang, and G. Li, “Recent progress in InGaN-based photodetectors for visible light communication,” *J. Mater. Chem. C* **10**, 14080–14090 (2022).
- ¹¹C. A. M. Fabien, A. Maros, C. B. Honsberg, and W. A. Doolittle, “III-Nitride Double-Heterojunction Solar Cells With High In-Content InGaN Absorbing Layers: Comparison of Large-Area and Small-Area Devices,” *IEEE J. Photovolt.* **6**, 460–464 (2016).
- ¹²S.-W. Feng, C.-M. Lai, C.-H. Chen, W.-C. Sun, and L.-W. Tu, “Theoretical simulations of the effects of the indium content, thickness, and defect density of the i-layer on the performance of p-i-n InGaN single homojunction solar cells,” *Journal of Applied Physics* **108**, 093118 (2010).
- ¹³Y. Zhang, M. J. Kappers, D. Zhu, F. Oehler, F. Gao, and C. J. Humphreys, “The effect of dislocations on the efficiency of InGaN/GaN solar cells,” *Solar Energy Materials and Solar Cells Dye Sensitized Solar Cells, Organic, Hybrid Solar Cells and New Concepts*, **117**, 279–284 (2013).
- ¹⁴U. Chatterjee, J.-H. Park, D.-Y. Um, and C.-R. Lee, “III-nitride nanowires for solar light harvesting: A review,” *Renewable and Sustainable Energy Reviews* **79**, 1002–1015 (2017).
- ¹⁵J. Kamimura, M. Ramsteiner, L. Geelhaar, and H. Riechert, “Si doping effects on (In,Ga)N nanowires,” *Journal of Applied Physics* **116**, 244310 (2014).
- ¹⁶X. Zhang, H. Lourenço-Martins, S. Meuret, M. Kociak, B. Haas, J.-L. Rouvière, P.-H. Jouneau, C. Bougerol, T. Auzelle, D. Jalabert, X. Biquard, B. Gayral, and B. Daudin, “InGaN nanowires with high InN molar fraction: growth, structural and optical properties,” *Nanotechnology* **27**, 195704 (2016).
- ¹⁷G. T. Wang, Q. Li, J. J. Wierer, D. D. Koleske, and J. J. Figiel, “Top-down fabrication and characterization of axial and radial III-nitride nanowire LEDs,” *Phys. Status Solidi A* **211**, 748–751 (2014).
- ¹⁸O. Brandt, Y. J. Sun, L. Däwritz, and K. H. Ploog, “Ga adsorption and desorption kinetics on M-plane GaN,” *Phys. Rev. B* **69**, 165326 (2004).
- ¹⁹C. S. Gallinat, G. Koblmüller, J. S. Brown, and J. S. Speck, “A growth diagram for plasma-assisted molecular beam epitaxy of In-face InN,” *Journal of Applied Physics* **102**, 064907 (2007).
- ²⁰D. N. Nath, E. Gür, S. A. Ringel, and S. Rajan, “Molecular beam epitaxy of N-polar InGaN,” *Applied Physics Letters* **97**, 071903 (2010).
- ²¹M. Schuster, P. O. Gervais, B. Jobst, W. Höslner, R. Averbeck, H. Riechert, A. Iberl, and R. Stömmmer, “Determination of the chemical composition of distorted InGaN/GaN heterostructures from x-ray diffraction data,” *J. Phys. D: Appl. Phys.* **32**, A56 (1999).
- ²²M. A. Moram and M. E. Vickers, “X-ray diffraction of III-nitrides,” *Rep. Prog. Phys.* **72**, 036502 (2009).
- ²³H. Chen, R. M. Feenstra, J. E. Northrup, T. Zywiets, J. Neugebauer, and D. W. Greve, “Surface structures and growth kinetics of InGaN(0001) grown by molecular beam epitaxy,” *J. Vac. Sci. Technol. B Microelectron. Nanometer Struct. Process. Meas. Phenom.* **18**, 2284–2289 (2000).
- ²⁴C. Chêze, F. Feix, M. Anikeeva, T. Schulz, M. Albrecht, H. Riechert, O. Brandt, and R. Calarco, “In/GaN(0001)-(3×3)R30° adsorbate structure as a template for embedded (In, Ga)N/GaN monolayers and short-period superlattices,” *Applied Physics Letters* **110**, 072104 (2017).
- ²⁵K. Hestroffer, F. Wu, H. Li, C. Lund, S. Keller, J. S. Speck, and U. K. Mishra, “Relaxed c-plane InGaN layers for the growth of strain-reduced InGaN quantum wells,” *Semicond. Sci. Technol.* **30**, 105015 (2015).
- ²⁶K. Hestroffer, C. Lund, H. Li, S. Keller, J. S. Speck, and U. K. Mishra, “Plasma-assisted molecular beam epitaxy growth diagram of InGaN on (0001)GaN for the optimized synthesis of InGaN compositional grades,” *Phys. Status Solidi B* **253**, 626–629 (2016).
- ²⁷S. Valdueza-Felip, E. Bellet-Amalric, A. Núñez-Cascajero, Y. Wang, M.-P. Chauvat, P. Ruterana, S. Pouget, K. Lorenz, E. Alves, and E. Monroy, “High In-content InGaN layers synthesized by plasma-assisted molecular-beam epitaxy: Growth conditions, strain relaxation, and In incorporation kinetics,” *Journal of Applied Physics* **116**, 233504 (2014).

- ²⁸C. Bazioti, E. Papadomanolaki, Th. Kehagias, T. Walther, J. Smalc-Koziorowska, E. Pavlidou, Ph. Kominou, Th. Karakostas, E. Iliopoulos, and G. P. Dimitrakopoulos, "Defects, strain relaxation, and compositional grading in high indium content InGaN epilayers grown by molecular beam epitaxy," *Journal of Applied Physics* **118**, 155301 (2015).
- ²⁹J. Moneta, M. Siekacz, E. Grzanka, T. Schulz, T. Markurt, M. Albrecht, and J. Smalc-Koziorowska, "Peculiarities of plastic relaxation of (0001) InGaN epilayers and their consequences for pseudo-substrate application," *Applied Physics Letters* **113**, 031904 (2018).
- ³⁰Z. Lv, H. Wang, and H. Jiang, "Surface Evolution of Thick InGaN Epilayers with Growth Interruption Time," *J. Phys. Chem. C* **125**, 16643–16651 (2021).
- ³¹H. Wang, D. S. Jiang, U. Jahn, J. J. Zhu, D. G. Zhao, Z. S. Liu, S. M. Zhang, Y. X. Qiu, and H. Yang, "Investigation on the strain relaxation of InGaN layer and its effects on the InGaN structural and optical properties," *Physica B: Condensed Matter* **405**, 4668–4672 (2010).
- ³²H. B. Bebb and E. W. Williams, *Transport and Optical Phenomena: Photoluminescence I: Theory*, edited by R. K. Willardson and A. C. Beer, Semiconductors and Semimetals, Vol. 8 (Academic Press, New York, 1972).
- ³³W. Shan, W. Walukiewicz, E. E. Haller, B. D. Little, J. J. Song, M. D. McCluskey, N. M. Johnson, Z. C. Feng, M. Schurman, and R. A. Stall, "Optical properties of $\text{In}_x\text{Ga}_{1-x}\text{N}$ alloys grown by metalorganic chemical vapor deposition," *Journal of Applied Physics* **84**, 4452–4458 (1998).
- ³⁴C. Weisbuch, S. Nakamura, Y.-R. Wu, and J. S. Speck, "Disorder effects in nitride semiconductors: impact on fundamental and device properties," *Nanophotonics* **10**, 3–21 (2021).
- ³⁵S. N. S. Nakamura and T. M. T. Mukai, "High-Quality InGaN Films Grown on GaN Films," *Jpn. J. Appl. Phys.* **31**, L1457 (1992).
- ³⁶D. S. Arteev, A. V. Sakharov, E. E. Zavarin, W. V. Lundin, A. N. Smirnov, V. Y. Davydov, M. A. Yagovkina, S. O. Usov, and A. F. Tsatsulnikov, "Investigation of Statistical Broadening in InGaN Alloys," *J. Phys.: Conf. Ser.* **1135**, 012050 (2018).
- ³⁷Z. Liliental-Weber, K. M. Yu, M. Hawkrige, S. Bedair, A. Berman, A. Emara, D. R. Khanal, J. Wu, J. Domagala, and J. Bak-Misiuk, "Structural perfection of InGaN layers and its relation to photoluminescence," *Phys. Status Solidi C* **6**, 2626–2631 (2009).

Growth of compositionally uniform $\text{In}_x\text{Ga}_{1-x}\text{N}$ layers with low relaxation degree on GaN by molecular beam epitaxy

Jingxuan Kang, Mikel Gómez Ruiz, Duc Van Dinh, Aidan F Campbell, Philipp John, Thomas Auzelle, Achim Trampert, Jonas Lähnemann, Oliver Brandt, and Lutz Geelhaar
Paul-Drude-Institut für Festkörperelektronik, Leibniz-Institut im Forschungsverbund Berlin e.V., Hausvogteiplatz 5–7, 10117 Berlin, Germany.

Supplementary Material

by Gallinat et al.²

A. Substrate temperature calibration by reflection high-energy electron diffraction

Prior to growth, the substrate temperature is calibrated by determining the desorption rate of In droplets. To this end, the intensity of the specular spot in the reflection high-energy electron diffraction (RHEED) pattern is recorded, as illustrated in Fig. S1(a) and reported previously.¹ A fixed In flux Φ_0 is provided which is sufficiently high to enable the accumulation of In droplets on the GaN(0001) surface. The corresponding evolution of the RHEED intensity is depicted in Fig. S1(b). Upon opening of the In cell shutter at the time 0, the RHEED intensity increases first and then steadily decreases during the formation of an In adlayer. Following the completion of the In adlayer at the time t_0 , excess In accumulates into droplets on top of the adlayer while the RHEED intensity remains constant. At the time t_1 (60 s in this study), the In cell shutter is closed, and the droplets are getting consumed by replenishing the adlayer, which is continuously desorbing. The RHEED intensity remains constant until the droplets have vanished. Subsequently, at time t_2 the adlayer desorbs and the RHEED intensity increases. During the adlayer desorption process, intensity oscillations may occur (as indicated by t_3) if a bilayer has formed. The mass balance for In droplet formation and desorption on the adlayer allows to determine the desorption rate Φ_{des} from equation 1 below. In turn, the In desorption rate is governed by the substrate temperature, and for our calibration we use the data reported

$$\Phi_{des} = \Phi_0 \times \frac{t_1 - t_0}{t_2 - t_0} \quad (1)$$

B. Structural analysis of the $\text{In}_{0.14}\text{Ga}_{0.86}\text{N}$ layer

The structural analysis of the $\text{In}_{0.14}\text{Ga}_{0.86}\text{N}$ layer corresponding to the photoluminescence spectrum centered at 2.87 eV in the main text was carried out in the same way as presented in detail there for the $\text{In}_{0.12}\text{Ga}_{0.88}\text{N}$ layer. The results are shown in Fig. S2. The reciprocal space map (RSM) in Fig. S2(a) reveals an In content of 0.14 and a strain relaxation degree of 20%. These values are confirmed from $2\theta - \omega$ scans at the 0002, 0004, $10\bar{1}2$, $10\bar{1}3$, $11\bar{2}2$, and $20\bar{2}1$ reflections. The In content profile in Fig. S2(b), measured by secondary ion mass spectrometry (SIMS), reveals an In content of 0.14 in accordance with the RSM result. A slight increase is observed after the growth of the first 100 nm of $\text{In}_x\text{Ga}_{1-x}\text{N}$. This increase is attributed to strain relaxation. The dark spots on the panchromatic cathodoluminescence (CL) spectroscopy intensity map in Fig. S2(c) correspond to a threading dislocation density of approximately $1.9 \times 10^9 \text{ cm}^{-2}$.

¹O. Brandt, Y. J. Sun, L. Däweritz, and K. H. Ploog, "Ga adsorption and desorption kinetics on M-plane GaN," *Phys. Rev. B* **69**, 165326 (2004).

²C. S. Gallinat, G. Koblmüller, J. S. Brown, and J. S. Speck, "A growth diagram for plasma-assisted molecular beam epitaxy of In-face InN," *Journal of Applied Physics* **102**, 064907 (2007).

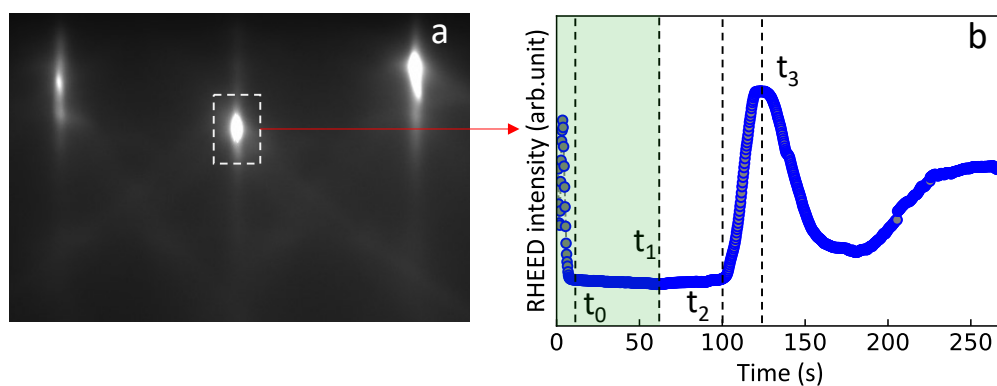


FIG. S1. (a) RHEED pattern of the GaN (0001) substrate surface along the $[1\bar{1}00]$ azimuth. The dashed rectangle marks the area around the specular spot whose intensity evolution during the temperature calibration process is shown in (b). The In shutter is open during the time indicated by the green shading. The times t_0 , t_1 , t_2 , and t_3 mark the completion of the In adlayer, the closing of the In shutter, the full desorption of the In droplets, and an oscillation associated with the desorption of the In adlayer.

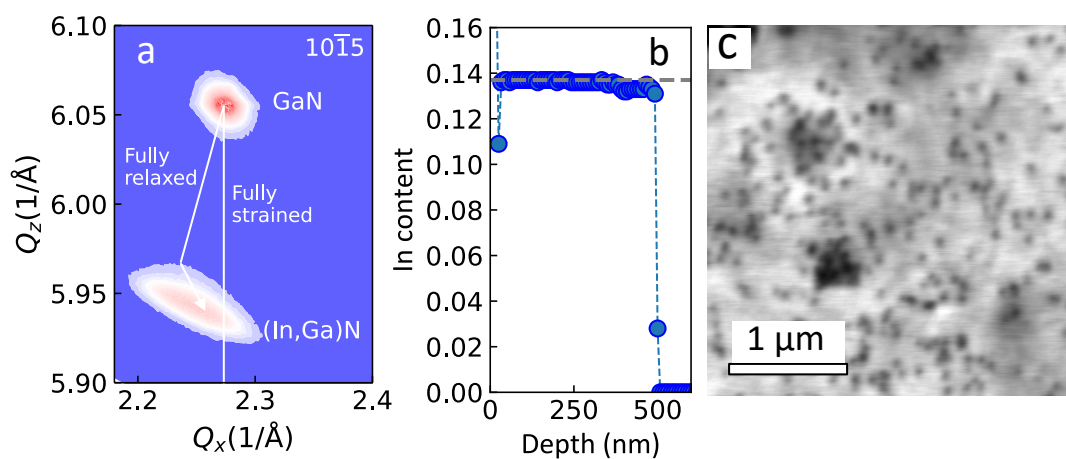


FIG. S2. Structural analysis of the $\text{In}_{0.14}\text{Ga}_{0.86}\text{N}$ layer. (a) RSM around the GaN $10\bar{1}5$ reflection. (b) In content depth profile obtained by SIMS. (c) Panchromatic CL intensity map acquired at 10 K.